SPATIALLY RESOLVED CHEMISTRY IN NEARBY GALAXIES. III. DENSE MOLECULAR GAS IN THE INNER DISK OF THE LIRG IRAS 04296+2923

DAVID S. MEIER[1,2], JEAN L. TURNER[3], AND SARA C. BECK[4]

[1] Department of Physics, New Mexico Institute of Mining and Technology, 801 Leroy Place, Socorro, NM 87801, USA; dmeier@nmt.edu
[2] National Radio Astronomy Observatory, P.O. Box O, Socorro, NM 87801, USA
[3] Department of Physics and Astronomy, UCLA, Los Angeles, CA 90095-1547, USA; turner@astro.ucla.edu
[4] Department of Physics and Astronomy, Tel Aviv University, 69978 Ramat Aviv, Israel; sara@wise.tau.ac.il

ABSTRACT

We present a survey of 3 mm molecular lines in IRAS 04296+2923, one of the brightest known molecular-line emitting galaxies, and one of the closest luminous infrared galaxies (LIRGs). Data are from the Owens Valley and CARMA millimeter interferometers. Species detected at $\lesssim 4''$ resolution include $C^{18}O$, HCN, HCO^+, HNC, CN, CH_3OH, and, tentatively, HNCO. Along with existing CO, ^{13}CO, and radio continuum data, these lines constrain the chemical properties of the inner disk. Dense molecular gas in the nucleus fuels a star formation rate $\gtrsim 10\ M_\odot\ yr^{-1}$ and is traced by lines of HCN, HCO^+, HNC, and CN. A correlation between HCN and star formation rate is observed on sub-kiloparsec scales, consistent with global relations. Toward the nucleus, CN abundances are similar to those of HCN, indicating emission comes from a collection (~ 40–50) of moderate visual extinction, photon-dominated-region clouds. The CO isotopic line ratios are unusual: $CO(1$–$0)/^{13}CO(1$–$0)$ and $CO(1$–$0)/C^{18}O(1$–$0)$ line ratios are large toward the starburst, as is commonly observed in LIRGs, but farther out in the disk these ratios are remarkably low ($\lesssim 3$). $^{13}CO/C^{18}O$ abundance ratios are lower than in Galactic clouds, possibly because the $C^{18}O$ is enriched by massive star ejecta from the starburst. ^{13}CO is underabundant relative to CO. Extended emission from CH_3OH indicates that dynamical shocks pervade both the nucleus and the inner disk. The unusual CO isotopologue ratios, the CO/HCN intensity ratio versus L_{IR}, the HCN/CN abundance ratio, and the gas consumption time versus inflow rate all indicate that the starburst in IRAS 04296+2923 is in an early stage of development.

Key words: astrochemistry – galaxies: individual (IRAS 04296+2923, 2MASX J04324860+2929578) – galaxies: ISM – galaxies: starburst – radio lines: galaxies

Online-only material: color figure

1. INTRODUCTION

Luminous infrared galaxies (LIRGs) and ultraluminous infrared galaxies (ULIRGs) represent the most active members of the star-forming galaxy population in the nearby universe. Often morphologically disturbed with vast reservoirs of atomic and molecular gas (e.g., Sanders et al. 1988, 1991; Solomon et al. 1997), their high IR luminosities are driven by prodigious amounts of efficient star formation (e.g., Sanders & Mirabel 1996). LIRGs are important laboratories for the interplay of molecular gas and starbursts and their evolution over time. However, local LIRGs are rare (e.g., Soifer et al. 1987; Sanders et al. 2003), so there are few examples that are near enough that we can detect and resolve their chemical properties.

Despite being one of the nearest (29 Mpc; 140 pc =1″) LIRGs, IRAS 04296+2923 [hereafter IRAS 04296]—located behind the dark cloud L1500 in Taurus—has remained poorly studied until recently (Meier et al. 2010). It was not so long ago that it was even identified as a galaxy (Strauss et al. 1992; Chamaraux et al. 1995). Within 35 Mpc only the galaxies NGC 1068, NGC 1365, NGC 2146, NGC 4418, and NGC 7552 are as IR luminous as IRAS 04296, at $\sim 10^{11} L_\odot$ (Table 1; Sanders et al. 2003). IRAS 04296 is remarkable for the compactness of its starburst, with an estimated star formation rate of $\sim 10\ M_\odot\ yr^{-1}$ originating within the central 2″ (<280 pc), and $\sim 25\ M_\odot\ yr^{-1}$ for the entire galaxy (Meier et al. 2010). CO mapping with the Owens Valley Millimeter Array (OVRO) revealed an extremely massive molecular gas disk of $M(H_2) \simeq 6 \times 10^9 M_\odot$ within the central 45″ (Meier et al. 2010). No galaxy within 30 Mpc, observed in the Five Colleges Radio Astronomy Observatory (FCRAO) CO survey (Young et al. 1995), has as high a CO luminosity over that aperture. Toward the central region H_2 column densities are $1 \times 10^{23}\ cm^{-3}$ averaged over 500 pc scales. IRAS 04296 is one of the most gas-rich systems in the nearby universe.

In many respects, IRAS 04296 appears to be "normal" bar-induced star formation taken to an extreme (Figure 1; Meier et al. 2010). Unlike many [U]/LIRGs, there are no obvious signs, morphological or kinematic, of a recent major merger. It is a symmetric, barred spiral galaxy with a pronounced outer "theta" ring. However, judging from the estimated gas inflow rates along the bar, IRAS 04296 is not in a stable configuration. The nuclear star formation rate is so large that the nuclear component is being consumed more rapidly than it can be replenished by the bar-driven inflow of $\sim 5\ M_\odot\ yr^{-1}$. This argues that IRAS 04296 is early in its LIRG state; the observed starburst can be maintained for the next 100 Myr (Meier et al. 2010).

IRAS 04296's unusual CO brightness raises questions about the dense gas in this LIRG. How much dense gas is there in IRAS 04296, and where is it found? What are the densities and temperatures of the gas clouds? What are the effects of the nuclear starburst on the dense gas? What are the effects of bar inflow on the dense gas? What does the dense gas and its chemistry reveal about the nuclear starburst in this LIRG? Here we use 3 mm aperture synthesis observations to address these questions in IRAS 04296. The target molecules are tracers of dense gas and probe a range of chemical conditions.

2. OBSERVATIONS

Aperture synthesis observations were obtained for IRAS 04296 in dense gas tracers at $\lambda = 3$ mm with the

Table 1
IRAS 04296+2923 Basic Data

Characteristic	Value	Reference
Dynamical Center[a]	$\alpha(2000) = 04^{\rm h}32^{\rm m}48\overset{s}{.}65 \pm 1''$	1
(kinematic)	$\delta(2000) = +29°29'57\overset{''}{.}45 \pm 1''$	
$2\,\mu$m Peak (2MASS)	$\alpha(2000) = 04^{\rm h}32^{\rm m}48\overset{s}{.}60 \pm 0\overset{''}{.}3$	1
	$\delta(2000) = +29°29'57\overset{''}{.}49 \pm 0\overset{''}{.}3$	
$V_{\rm lsr}$[a]	2086 km s^{-1}	1
Adopted Distance	29 Mpc	1
Position Angle[a]	252°	1
Inclination	50°	1
$M_{H_2}(<3\overset{''}{.}5)$[b]	$4.3 \times 10^8 M_\odot$	1
$\Sigma_{H_2}(<3\overset{''}{.}5)$[b]	550 $M_\odot$ pc^{-2}	1
$M_{\rm dyn}(<3\overset{''}{.}5)$[a]	$1.6 \times 10^9 M_\odot$	1
$M_{H_2}(<30'')$[c]	$5.9 \times 10^9 M_\odot$	1
$M_{\rm dyn}(<30'')$[a]	$3.0 \times 10^{10} M_\odot$	1
$M_{\rm HI}^{\rm tot}$	$1.38 \times 10^9 M_\odot$	3
IRAS $12\mu, 25\mu, 60\mu, 100\mu$	1.39, 5.90, 42.1, 48.3 Jy	2
$L_{\rm IR}$	$9.8 \times 10^{10} L_\odot$	2

Notes.
[a] Based on the best-fitting rotation curve.
[b] From ^{13}CO(1–0).
[c] Assuming the standard CO conversion factor.
References. (1) Meier et al. (2010); (2) Sanders et al. (2003); (3) Chamaraux et al. (1995).

Combined Array for Research in Millimeter Astronomy (CARMA; Woody et al. 2004). Table 2 lists the molecular transitions surveyed along with their observational parameters. Observing parameters for data from the Owens Valley Millimeter Array (OVRO: Scoville et al. 1994) consisting of transitions between 109 and 113 GHz are as reported in Meier et al. (2010). The CO(1–0) and ^{13}CO(1–0) observations have a velocity resolution of 10.5 km s^{-1}. The lines presented here were observed simultaneously in wideband mode (128×31.25 MHz) giving a velocity resolution of ~ 90 km s^{-1}. The 88–97 GHz tuning was observed separately with the CARMA interferometer but had the same wideband 31.25 MHz channels ($v_{\rm chan} \sim 100$ km s^{-1}). All detected lines are resolved spectrally (emission in at least three adjacent channels) toward the nucleus, but the low spectral

resolution may imply some spectral "beam dilution" toward the narrower line width disk.

The OVRO and CARMA data sets were calibrated using the MMA and MIRIAD software packages, respectively. Phase calibration was done by observing the quasar J0336+323 every 25 minutes (OVRO) and 0237+288 or 0530+135 every 20 minutes (CARMA). Absolute flux calibration was done using Uranus as primary flux calibrator and 3C273, 3C84, and 3C454.3 for secondary flux calibration (both OVRO and CARMA). Uncertainties in absolute flux calibration are $\sim 10\%$ for both data sets. Mapmaking was done in MIRIAD and subsequent data analysis and manipulation was done with the NRAO AIPS package. All data were naturally weighted. Spatial resolutions are $\lesssim 4\overset{''}{.}5$ for the high frequency (OVRO) tuning and $\lesssim 3\overset{''}{.}3$ for the low frequency (CARMA) tuning. Integrated intensity images are moment 0 maps with all emission brighter than 1.3σ per channel included. Since the emission observed from these higher density tracers remain confined well inside the half power point of the array(s), corrections for the primary beam attenuation have not been applied. No single-dish observations of this galaxy exists for these transitions, so no estimate of the amount of resolved-out flux is possible; however, it is not expected that there is missing flux as it would require the existence of a uniform dense component extended on $\gtrsim 6$ kpc scales.

3. RESULTS: INTEGRATED INTENSITY MAPS AND ABUNDANCES

Figure 2 displays the integrated intensity maps of the detected transitions along with ^{12}CO(1–0) and ^{13}CO(1–0) from Meier et al. (2010). The CO(1–0) intensity map displays the overall structure of IRAS 04296. Two barred arms extend from the outer, low pitch angle spiral arms into the central region where the gas collects into a very bright nuclear feature, referred to as the circum-nuclear zone (CNZ). The CNZ has a radius, corrected for inclination, $\simeq 0.9$ kpc (Meier et al. 2010). The CNZ region is also the site of an intense starburst which dominates the radio continuum and mid-infrared emission (Meier et al. 2010). The compact core of the starburst traced with 6 cm radio continuum (marked in Figure 2 by a cross) is confined to the inner $3''$ or ~ 200 pc radius. The centroid of this compact starburst is close to

Table 2
Observational Data

Transition	Dates (MMYY)	Frequency (GHz)	$T_{\rm sys}$ (K)	$\Delta V_{\rm chan}$ (km s^{-1})	Beam ($''\times''$;°)	K/Jy	Noise (mJy bm^{-1})
CARMA[a]:							
HCN(1–0)	0808–1008	88.632	130–230	105.7	$3.3 \times 2.7; -90$	17.5	2.9
HCO$^+$(1–0)		89.189		105.0		17.3	2.9
HNC(1–0)		90.664		103.3		16.7	2.9
C^{34}S(2–1)		96.413		97.17		14.8	3.0
CH$_3$OH(2_k–1_k)		96.741		96.84		14.7	3.0
OVRO[b]:							
HC$_3$N(12–11)	1103–0504	109.174	220–450	85.8	$4.7 \times 3.8; -15$	5.91	4.0
C^{18}O(1–0)[c]		109.782		85.3		5.86	4.0
HNCO(5_{05}–4_{04})[c]		109.905					
CN(1–0; $\frac{3}{2}-\frac{1}{2}$)		113.491		82.5	$4.6 \times 3.6; -14$	5.71	4.5
CN(1–0; $\frac{1}{2}-\frac{1}{2}$)[d]		113.191					

Notes.
[a] Phase Center: $\alpha = 04^{\rm h}32^{\rm m}48\overset{s}{.}6$ $\delta = +29°29'57\overset{''}{.}5$ (J2000).
[b] Phase Center: $\alpha = 04^{\rm h}32^{\rm m}48\overset{s}{.}6$ $\delta = +29°29'58\overset{''}{.}0$ (J2000).
[c] Partially blended.
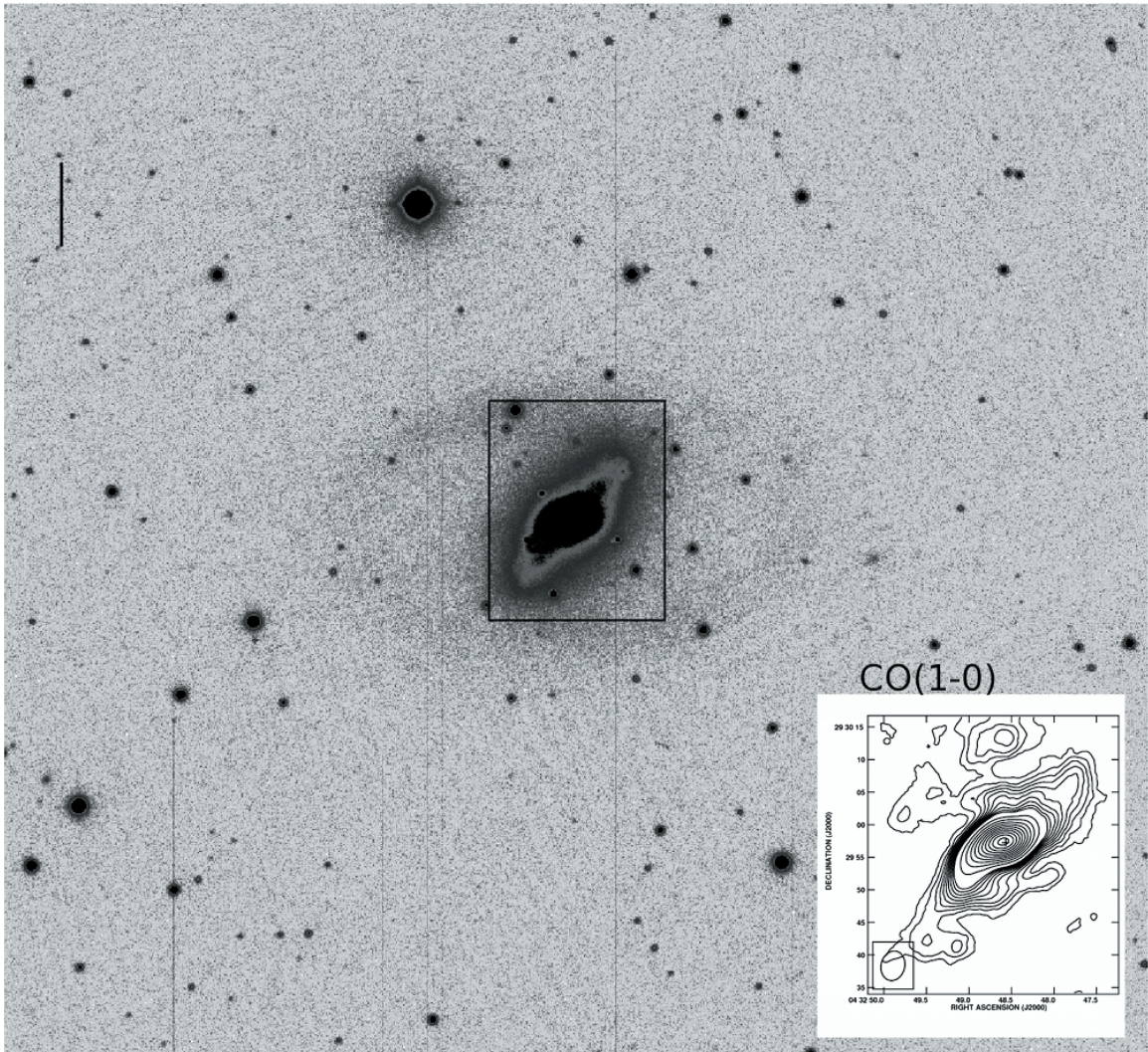[d] Observed simultaneously with CN(1–0; $3/2 - 1/2$).

Figure 1. *J*-band near infrared image of IRAS 04296 from the Palomar 5 m with CO(1–0) integrated intensity in the bottom right corner (Meier et al. 2010). The black box marks the field of view covered in CO(1–0). Contours are 1, 2, 3, ... 10, 15, 20, ... 60 ×13.8 K km s^{-1} for a beam size of $4\rlap{.}''6 \times 3\rlap{.}''6; -14°$ (Meier et al. 2010). The scale bar in the upper left is 2.8 kpc ($20''$) long.

the center of the CNZ dense gas distribution, but appears shifted slightly ($\sim 1''$) southwest of the centroid of the CO. Somewhat weaker star formation traced by 20 cm radio continuum matches the extent of the CNZ (see section 4.2.3). Beyond the CNZ, CO emission extends out to a galactocentric radius of $\sim 25''$ or ~ 3.5 kpc. CO(1–0) from the outermost portion of the field, including the separate northernmost clump, originates in the outer spiral arms.

Below, we discuss the morphology of each dense gas transition. In the following sections, we adopt an excitation temperature of $T_{ex} = 30$ K for the nucleus and $T_{ex} = 10$ K for the bar and arms. These are probably reasonable estimates given that the starburst is strongly localized to the nucleus. However, until multi-line studies can be executed, these should be considered "reference values" only.

C^{18}O(1–0) and HNCO(5$_{05}$–4$_{04}$)—The C^{18}O(1–0) and HNCO(5$_{05}$–4$_{04}$) transitions appear together in the same spectral window. The transitions are separated by about 330 km s^{-1}, so may potentially be blended, but the velocity field of the galaxy and the faintness of HNCO allows C^{18}O(1–0) to be unambiguously separated. C^{18}O(1–0) is surprisingly extended. Like the (continuum subtracted) ^{13}CO(1–0), C^{18}O(1–0) peaks just southeast of the starburst. The CNZ is not significantly brighter than

the arms in C^{18}O(1–0), remarkably different from CO(1–0), where it is more than an order of magnitude stronger. This would be consistent with higher cloud temperatures in the CNZ, which would increase the intensity of optically thick CO. Along the arms, C^{18}O(1–0) brightnesses are comparable to ^{13}CO(1–0). At the northern bar end, ^{13}CO(1–0) intensities increase slightly compared to C^{18}O. Peak brightnesses reach 0.10 K averaged over ~ 0.5 kpc scales near the starburst and close to this along the northern arm. C^{18}O column densities are discussed in detail below (Section 4.1).

HNCO(5$_{05}$–4$_{04}$) is tentatively detected ($\sim 3\sigma$) only in the western CNZ. For $T_{ex} = 30$ K, the HNCO column densities peak at N(HNCO) $\lesssim 2.3 \times 10^{14}$ cm^{-2}. Increasing T_{ex} to 50 K would raise the N(HNCO) limit to 4.1×10^{14} cm^{-2} (Table 3).

HCN(1–0), HCO$^+$(1–0), and HNC(1–0)—All three of these dense gas tracers are bright and compact. HCN(1–0) is the brightest with antenna temperatures peaking at 0.94 K, while HCO$^+$(1–0) and HNC(1–0) are $\sim 15\%$ and $\sim 50\%$ fainter, respectively. HCN(1–0) and HCO$^+$(1–0) peak toward the starburst but extend beyond it to cover the entirety of the CNZ (Figure 3). The dense gas tracers have abundances ranging from 3.3–5.4×10^{-9} here, assuming optically thin emission, with HNC and HCO$^+$ at the low end and HCN at the high end.

3

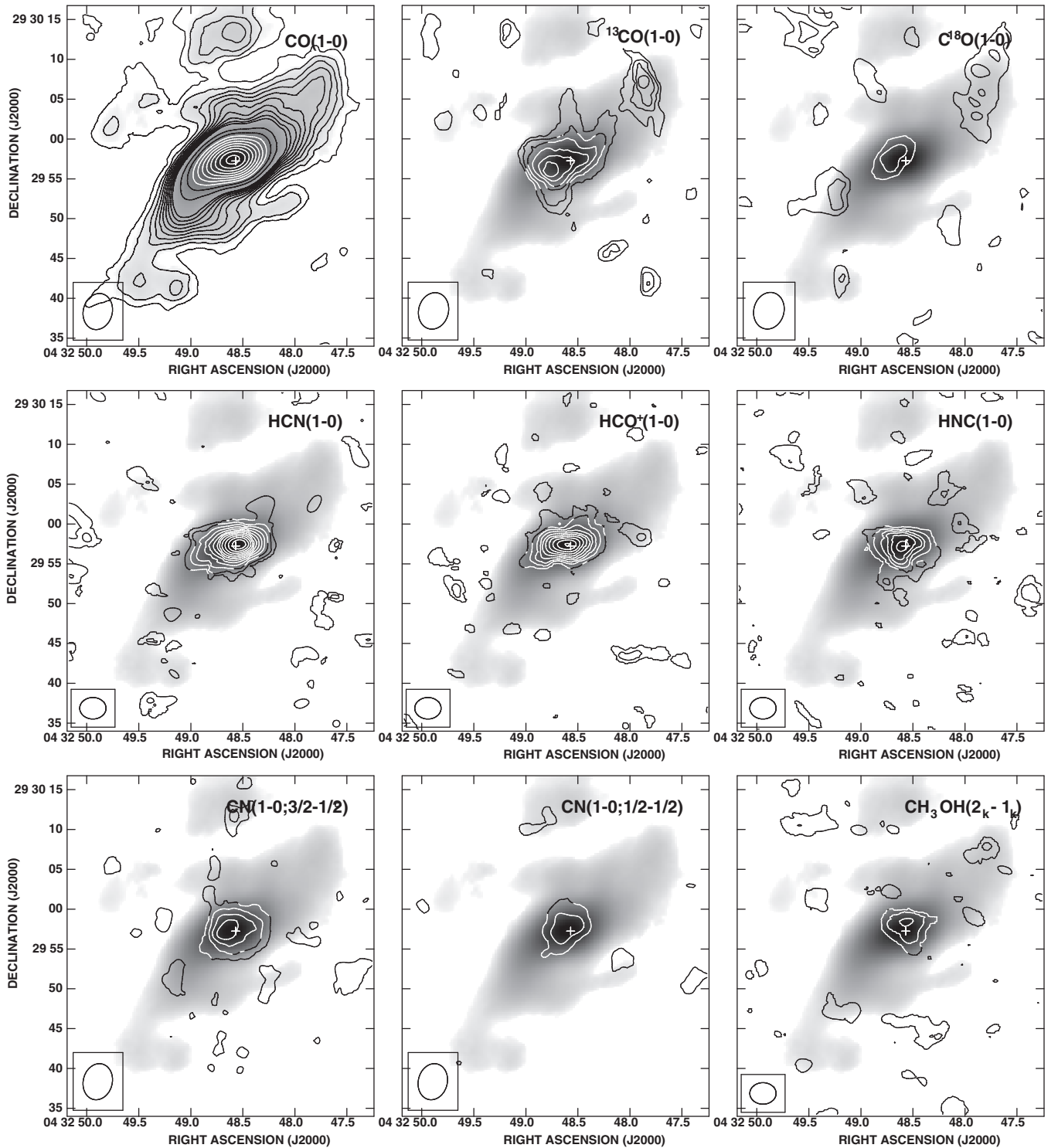**Figure 2.** Integrated intensity maps of the seven detected transitions, plus CO(1–0) in grayscale and ^{13}CO(1–0). The latter two are from Meier et al. (2010). The beam of all transitions is displayed in the lower left of each panel, and the cross marks the location of the starburst (radio continuum peak; Meier et al. 2010). Top Left: CO(1–0). Contours are 1, 2, 3, ... 10, 15, 20, ... 60 $\times 13.8$ K km s^{-1} for a beam size of $4\rlap{.}''6 \times 3\rlap{.}''6$; $-14°$. Top Center: ^{13}CO(1–0). Contour levels are 7.3 K km s^{-1} for the same beam size as CO(1–0). Beam sizes for the remaining transitions are as listed in Table 2. Top Right: C^{18}O(1–0). Contours as for ^{13}CO(1–0). Middle Left: HCN(1–0). Contour levels are 13.1 K km s^{-1}. Middle Center: HCO$^+$(1–0). Contour levels are 17.3 K km s^{-1}. Middle Right: HNC(1–0). Contours levels 16.7 K km s^{-1}. Bottom Left: CN(1–0; (3/2) − (1/2)). Contours levels are 12.8 K km s^{-1} Bottom Center: CN(1–0; (1/2) − (1/2)). Contours as for CN(1–0; (3/2) − (1/2)). Bottom Right: Combined intensity for the CH$_3$OH($2_k - 1_k$) quadruplet lines. Contours levels are 16.2 K km s^{-1}. The above contours correspond approximately to 2σ increments for each transition except CO(1–0) (see Table 1).

For HNC and HCO$^+$, abundances are higher than usual for single-dish measurements toward nearby star forming galaxies (Huettemeister et al. 1995; Nguyen-Q-Rieu et al. 1992), but typical of higher-resolution interferometer values (Seaquist et al. 1998; Kohno et al. 2001; Meier & Turner 2005; Knudsen et al. 2007; Meier & Turner 2012). Very weak emission is detected in HCN at two locations along the arms but clear emission is not detected in HCO$^+$ and HNC. The CO/HCN
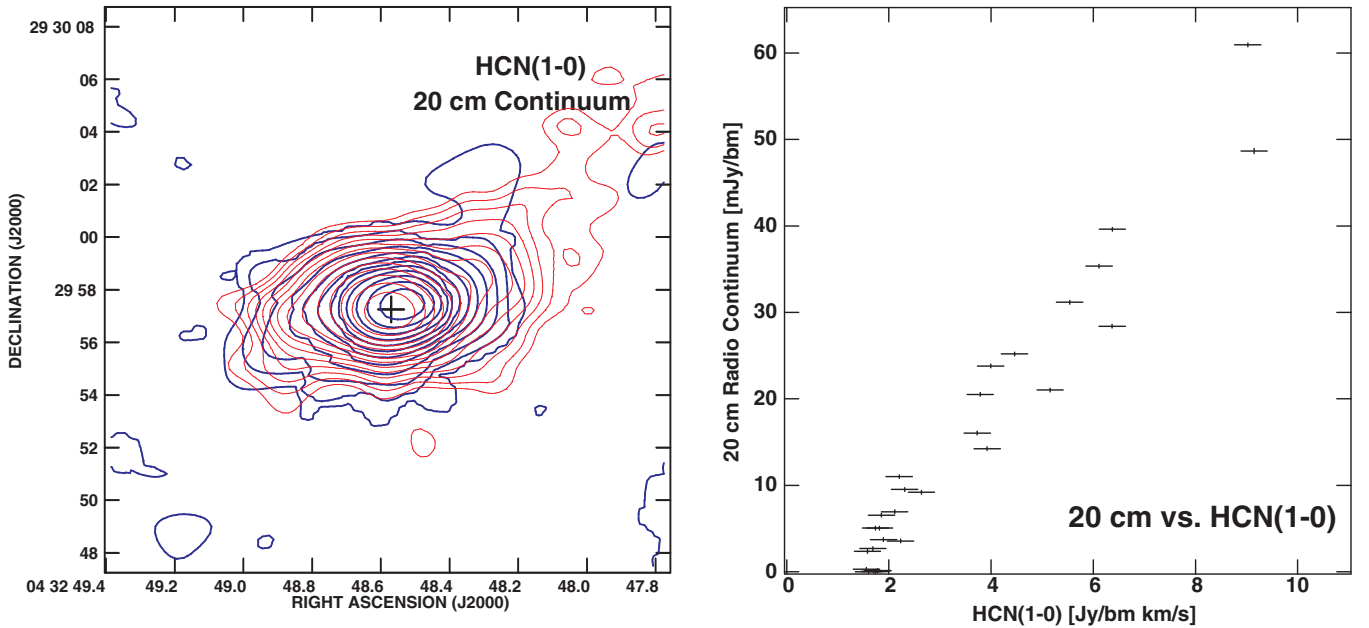
Figure 3. Left: the HCN(1–0) integrated intensity maps overlaid on high-resolution 20 cm radio continuum (Meier et al. 2010). Contours for HCN(1–0) are blue lines and are as in Figure 2. Contours of 20 cm radio continuum are red lines in steps of $2^{n/2}$, n = 0,1,2 ... × 0.25 mJy beam^{-1} for a resolution of $1\farcs6 \times 1\farcs3$. Right: the pixel by pixel correlation between HCN(1–0) and the 20 cm continuum. The 20 cm image has been convolved to the same beam size as the HCN(1–0) data and then sampled in $1\farcs5$ (∼ half beam) intervals. Note that this sampling interval is smaller than the beam and so different plotted points are correlated. Points with upper limits for both 20 cm and HCN(1–0) have been suppressed.

(A color version of this figure is available in the online journal.)

Table 3
Molecular Abundances[a]

Species	CNZ/Starburst[b]	Northern Arm[c]
N(H₂)	$1.0 \times 10^{23\,d}$	$3.8 \times 10^{22\,e}$
HCN	5.6×10^{-9}	5.3×10^{-10}
HNC	3.3×10^{-9}	$<6.3 \times 10^{-10}$
CN	9.0×10^{-9}	$<2.2 \times 10^{-9}$
HCO⁺	3.4×10^{-9}	$<3.4 \times 10^{-10}$
C³⁴S	$<7.7 \times 10^{-10}$	$<1.1 \times 10^{-9}$
HC₃N	$\lesssim 5.6 \times 10^{-10}$	$<3.4 \times 10^{-10}$
CH₃OH	2.3×10^{-8}	$\sim 1.4 \times 10^{-8}$
HNCO	$\lesssim 2.3 \times 10^{-9}$	$<1.7 \times 10^{-9}$

Notes.
[a] All upper limits are 2σ.
[b] Assumes an excitation temperature of 30 K for all transitions and optically thin emission.
[c] Measured at $\alpha = 04^h 32^m 47\fs 9$; $\delta = +29°30'07''$ (J2000) and assumes an excitation temperature of 10 K for all transitions.
[d] Based on the N(C¹⁸O) value, a favored nuclear [CO/C¹⁸O] isotopologue ratio of 200 (Section 4.1.1) and CO/H₂ = 8.5 × 10⁻⁵ (Frerking et al. 1982).
[e] As in d, except for the favored northern bar value of [CO/C¹⁸O] isotopologue ratio of 225 (Section 4.1.2).

contrast ratio between nucleus (7–9) and arms (6–9) is similar (Section 4.2.1).

CN(1–0; 3/2–1/2) and CN(1–0; 1/2–1/2)—CN(1–0; 3/2–1/2) is dominated by the CNZ. Faint emission is tentatively detected along the southeast arm and the northernmost clump, but not in the northwestern arm. Both fine structure components of CN(1–0) are clearly detected toward the CNZ. Hyperfine structure is not resolved due to the low spectral resolution of the data. The CN(3/2–1/2)/CN(1/2–1/2) intensity ratio is 1.8 ± 0.5 matching the optically thin theoretical value

of 2, within uncertainties. For a $T_{ex} = 30$ K, peak CN column densities are N(CN) = 9.0×10^{14} cm^{-2}.

CH₃OH(2_k–1_k)—This line is composed of four transitions, (2_{-12}–1_{-11}) E, (2_{02}–1_{01}) A++, (2_{02}–1_{01}) E, and (2_{11}–1_{10}) E, which are blended in these spectra. We refer to the combined spectral feature as the 2_k–1_k transition of methanol. Unlike the dense gas tracers, CH₃OH(2_k–1_k) does not peak exactly at the starburst, but slightly to the north. Emission is tentatively detected from the bar ends. CH₃OH abundances are $X(\mathrm{CH_3OH}) \simeq 2.3 \times 10^{-8}$ toward the CNZ and within 50 % of this value at the ends of the bar. These abundances are quite large, reaching values comparable to the highest values seen on ∼50 pc scales toward strong bar shocks in nearby spirals (e.g., Meier & Turner 2005, 2012).

Non-detections—HC₃N(12–11) and C³⁴S(2–1) were searched for but not clearly detected anywhere across the field. There is tentative evidence for HC₃N(12–11) from the western CNZ but we do not consider it a detection. Upper limits for HC₃N(12–11)/HCN(1–0) and C³⁴S(2–1)/HCN(1–0) are $\lesssim 0.086$ and <0.064 (2σ), respectively. Abundance limits (for $T_{ex} = 30$ K) are $\lesssim 5.6 \times 10^{-10}$ and $<7.7 \times 10^{-10}$ for HC₃N and C³⁴S, respectively. For C³⁴S(2–1) this abundance is only weakly constraining, implying $X(CS) < 2 \times 10^{-8}$ for a ³²S/³⁴S isotopic ratio of ∼24 (e.g., Chin et al. 1996). Implied HC₃N abundance limits are ∼3–5 times lower than toward IC 342 (Meier et al. 2011), but similar to abundances observed for M 82 and Maffei 2 (Aladro et al. 2011a; Meier & Turner 2012).

4. DISCUSSION

4.1. ¹³CO and C¹⁸O as Probes of CO Gas Opacity and Column

The CO isotopologues ¹³C¹⁶O ("¹³CO") and ¹²C¹⁸O ("C¹⁸O") are valuable probes of opacity and isotopic abundance when compared to the most abundant isotopologue, ¹²C¹⁶O ("CO"). Under the LTE approximation, the isotopic ratios provide a
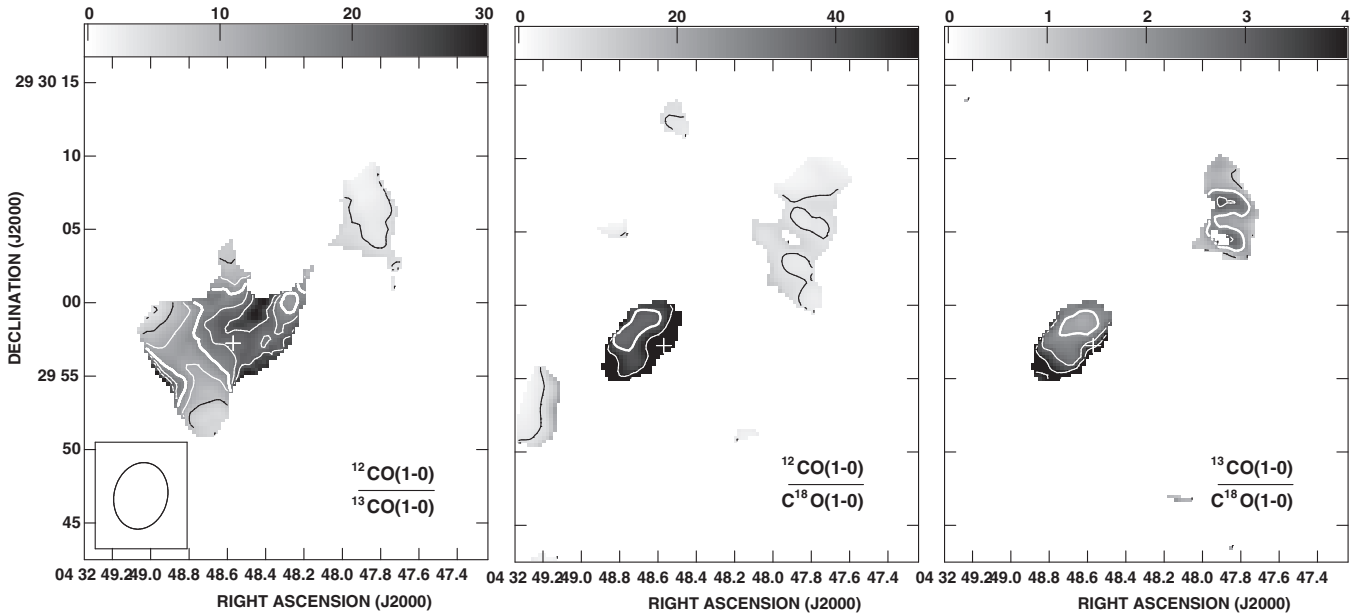
Figure 4. CO isotopologue ratios for IRAS 04296. Left: the CO(1–0)/^{13}CO(1–0) line ratio (Meier et al. 2010). Contours are 4, 8, 12, 16 (bold contour), 20, and 24. The grayscale ranges from 0 to 30 with dark being high ratios. Center: the CO(1–0)/C^{18}O(1–0) intensity ratio with the CO(1–0) data from (Meier et al. 2010). Contours are 6, 40 (bold contour), and 50. The grayscale ranges from 0 to 50 with dark being high ratios. Right: the ^{13}CO(1–0)/C^{18}O(1–0) intensity ratio with the ^{13}CO(1–0) data from (Meier et al. 2010). Contours are 1, 2 (bold contour), 3, and 4. The grayscale ranges from 0 to 4 with dark being high ratios. The beam size of all plots are the same and are given in the lower left of the figure.

direct constraint on gas opacity:

$$\mathbb{R}_i \simeq \frac{(1 - e^{-^{12}\tau})}{(1 - e^{-^{i}\tau})}, \qquad (1)$$

where $^{12}\tau$ is the CO(1–0) optical depth and $^{i}\tau$ is the CO(1–0) isotopologue optical depth ($^{13}\tau$ and $^{18}\tau$; e.g., Aalto et al. 1995). The lower opacity of the isotopologues also allow us to study the bulk of the molecular gas that is not sampled by optically thick CO. Furthermore, comparisons of the isotopologues with CO constrain gas opacity and isotopic abundance ratios and can reveal non-LTE gas excitation (e.g., Meier et al. 2000; Meier & Turner 2004). Typical values for the $\mathbb{R}_{13} \equiv$ CO(1–0)/^{13}CO(1–0) line intensity ratio range from $\mathbb{R}_{13} \sim 4$–7 for Galactic disk clouds; this range reflects both opacity effects and isotopic abundance ratios varying from [CO/^{13}CO] ~ 25–90 within the Galaxy. The inferred isotopic abundance ratio, [CO/^{13}CO], has its lowest values in the Galactic center and increases with galacto-centric radius, reaching ~ 70 at the solar circle and $\gtrsim 120$ in the outer Galaxy (e.g., Wilson & Rood 1994; Milam et al. 2005; Wouterloot & Brand 1996). A similar gradient is observed in the Galaxy for [CO/C^{18}O], with [CO/C^{18}O] ~ 250 at the Galactic Center and ~ 500 at the solar radius. This implies [^{13}CO/C^{18}O] between 6 and 10 across the Galaxy. In external galaxies, a wider range is seen, $\mathbb{R}_{13} \sim 3$–>30, with the higher values tending to originate from LIRGs and ULIRGs (Aalto et al. 1991; Casoli et al. 1992; Aalto et al. 1995). Typical values for the $\mathbb{R}_{18} \equiv$ CO(1–0)/C^{18}O(1–0) line intensity ratio are $\mathbb{R}_{18} \sim$ 15–100. ^{13}CO(1–0)/C^{18}O(1–0) intensity ratios, denoted $\mathbb{R}_{1318}$, tend to be lower than the Galactic [^{13}CO/C^{18}O], having values of 3–6 (e.g., Aalto et al. 1995).

Figure 4 presents the three isotopic line ratios, $\mathbb{R}_{13}$, $\mathbb{R}_{18}$, and $\mathbb{R}_{1318}$. All three exhibit the same trend that they are high toward the CNZ and lower along the arms. $\mathbb{R}_{13}$ is 16 ± 4 toward the CNZ but only 1.9 ± 0.4 at the north end of the northern arm (see Table 3 for position). Along the inner part of the bar arms

$\mathbb{R}_{13} \simeq 3$–4. Likewise, $\mathbb{R}_{18} = 45 \pm 10$ toward the CNZ and drops to 3.3 ± 0.7 by the end of the northern arm. The double rare isotopic ratio $\mathbb{R}_{1318}$, is fairly low everywhere across the mapped region, being 3.2 ± 0.7 toward the CNZ and falling to $\mathbb{R}_{1318} \simeq 1.7 \pm 0.5$ by the end of the northern bar. Toward the starburst site, $\mathbb{R}_{13}$ ($\mathbb{R}_{18}$) is 21 ± 4 (94 ± 30), even larger than seen elsewhere in the CNZ. However, $\mathbb{R}_{1318}$ is not significantly altered at the starburst ($\mathbb{R}_{1318} = 3.7 \pm 1.3$).

The elevated $\mathbb{R}_{13}$ and $\mathbb{R}_{18}$ ratios in the CNZ are not unexpected, since this has long been seen in starburst regions (e.g., Aalto et al. 1991; Casoli et al. 1992). Common explanations for the elevated $\mathbb{R}_{13}$ and $\mathbb{R}_{18}$ include, (1) lowered gas opacity due to broader line widths that result in lower CO column densities per unit velocity, (2) non-LTE effects that raise CO brightness relative to the isotopologues, such as sub-thermal gas densities or PDR/externally heated clouds, or (3) anomalous isotopic abundances.

In contrast, the low isotopic line ratios seen toward the bar arm imply (for LTE) high opacities. The isotopic ratios approach unity in the limit of infinite opacity. For Galactic local interstellar medium (ISM) abundance ratios (e.g., Wilson & Rood 1994), $^{18}\tau \gtrsim 1$ would be required to explain the very low $\mathbb{R}_{1318}$ values seen along the bar arms. However, such an interpretation conflicts with the other two ratios. If gas opacity is high enough to explain $\mathbb{R}_{1318}$, then both $\mathbb{R}_{13}$ and $\mathbb{R}_{18}$ should exhibit ratios much closer to unity. The observed $\mathbb{R}_{13}$ and $\mathbb{R}_{18}$ along the northwestern arm, while lower than toward the nucleus, are still significantly above unity.

Possible explanations for these unusual ratios for the nucleus and the bar arms are discussed below.

4.1.1. Low Opacity and Columns Toward the Circum-nuclear Zone

The high ratios toward the CNZ are not extreme compared to other LIRGs and imply low-opacity CO gas. A range of LTE solutions for gas opacity and isotopic abundance are possible. The optical depth of CO(1–0), $^{12}\tau$, can range from

$\simeq 4.0$, (corresponding to $[CO/^{13}CO] \simeq 60$, and $[CO/C^{18}O] \simeq 200$) to $\simeq 8.0$, (for $[CO/^{13}CO] \simeq 120$ and $[CO/C^{18}O] \simeq 375$). Pushing $^{12}\tau$ larger than 8.0 requires very large $[CO/^{13}CO]$ abundance ratios, greater than 120. These values would be consistent with the low nuclear processing levels observed for gas in the outermost parts of the Galaxy, based on the Wilson & Rood (1994) extrapolated gradient (there are indications that this gradient may be too shallow in the far-outer Galaxy; Wouterloot & Brand 1996), and with values of $[^{12}C/^{13}C] \sim 100$ recently suggested for the centers of local starburst galaxies (Martín et al. 2010; Henkel et al. 2014). On the other hand, pushing $^{12}\tau$ lower than 4.0 requires $[CO/C^{18}O]$ abundance ratios lower than seen anywhere in the Galaxy and lower than the fully massive star enriched values predicted from chemical evolution models (Henkel & Mauersberger 1993). Toward the starburst site, these constraints are even more dramatic if LTE applies (see below). Overall, low values of $^{12}\tau$ are favored for the CNZ based on a comparison with the northern arm (Section 4.1.2).

Low CO opacities in CO-bright nuclear starburst may seem surprising. Even ^{13}CO has moderate, not low opacity in the more normal spirals, IC 342 and Maffei 2 (Wall & Jaffe 1990; Meier et al. 2000; Meier & Turner 2001; Meier et al. 2008). The presence of the starburst and its location at the center of a barred potential alters the situation somewhat: the CO line width of the nuclear emission is about twice the line widths of the bar ends. The broader line accounts for some of the increased CO intensity toward the nucleus, but not all. The $C^{18}O$ peak brightness temperatures toward the CNZ and the northern arm differ by less than a factor of two.

Non-LTE effects can also be responsible for the high $\mathbb{R}_{13}$ and $\mathbb{R}_{18}$ values, especially toward the starburst. The $CO(1-0)/HCN(1-0)$ and $HCN(1-0)/HCO^{+}(1-0)$ line ratios over the CNZ argue that the gas is dense enough that sub-thermal CO emission can be neglected across the nucleus (Section 4.2.2). However, the chemical data indicate that the nuclear molecular emission may be partially influenced by photon-dominated regions (PDRs; Section 4.3). The radiation field from the starburst can heat the surfaces of the nearby clouds, preferentially exciting the optically thick (^{12}CO) transitions relative to the optically thin ^{13}CO and $C^{18}O$. The high radiation fields can also preferentially photo-dissociate the optically thinner species. Both mechanisms raise $\mathbb{R}_{13}$ and $\mathbb{R}_{18}$ relative to their values in quiescent conditions (e.g., Meier et al. 2000). Since ^{13}CO is not highly opaque, there should be a much weaker influence on $\mathbb{R}_{1318}$. Non-LTE effects are able to explain the elevated ratios toward the starburst relative to the CNZ, but must be extreme to change the conclusion that the CNZ has modest $^{12}\tau$.

So even accounting for non-LTE effects associated with the starburst, it appears that the observed nuclear CO isotopic line ratios imply quite low ^{13}CO opacities $^{13}\tau \ll 1$, $[CO/^{13}CO] \geqslant 60$ and $[CO/C^{18}O] \gtrsim 200$. The isotopic abundances ratios are consistent with an ISM enriched in ^{18}O from recent massive star ejecta. Moreover, a relatively lower abundance of ^{13}C suggests less long term nuclear processing, since C is a primary and ^{13}C is a (mostly) secondary nucleus (Henkel & Mauersberger 1993).

Adopting $[CO/C^{18}O] \simeq 200$ and an excitation temperature of 30 K along with a CO/H_2 abundance ratio of 8.5×10^{-5} (Frerking et al. 1982), we derive an H_2 column density of $N(H_2) \simeq 1.0 \times 10^{23}$ cm^{-2} toward the CNZ. This is about a factor of two lower than predicted based on a Galactic conversion factor of 2.0×10^{20} cm^{-2} (K km s^{-1})$^{-1}$ (Hunter et al. 1997; Strong et al. 1988). The Galactic conversion factor can be accommodated either by adopting a nuclear excita-

tion temperature of ~ 50 K over ~ 200 pc scales, or raising $[CO/C^{18}O]$ to ~ 340.

4.1.2. Anomalous ^{13}CO and $C^{18}O$ Ratios Across the Bar Arms

Toward the bar arms, the isotopic line ratios are very low compared to what is typically observed for disks in other extragalactic systems (e.g., Paglione et al. 2001). Under LTE, low $\mathbb{R}_{13}$ and $\mathbb{R}_{18}$ imply large $^{12}\tau$ (~ 65–110). It is counter-intuitive that the northern arm would have gas opacity at least an order of magnitude larger than the CNZ, while its CO intensity is more than an order of magnitude fainter. For these high opacities, the observed $\mathbb{R}_{1318}$ imply $[^{13}CO/C^{18}O] \sim 2.1$, which is lower than favored for the CNZ and more than three times lower than found in either the local Galactic ISM or the Galactic center region.

Assuming LTE it is difficult to obtain a consistent solution for these line ratios. To simultaneously match the three ratios at the end of the northern arm, we require $[CO/^{13}CO] \simeq 90$–140 (unusually high) and $[CO/C^{18}O] \simeq 185$–300, as $^{12}\tau$ ranges from 65 to 110. Given the strong bar here it is possible that the radial inflow of relatively unprocessed outer disk gas could explain the high $[CO/^{13}CO]$ ratio observed for the bar arms, however this explanation would imply that the $[CO/C^{18}O]$ abundance ratio should also be raised, which is not observed. These $[CO/^{13}CO]$ ratios suggest that stellar processing on the longer timescales typical of intermediate-mass star lifetimes is rather low.

If we accept the high end of the opacity range for the CNZ and the low end of the range for the end of the northern arm (to minimize dramatic opacity differences) then the implied abundance ratios $[CO/^{13}CO]$ and $[CO/C^{18}O]$ would both decline with galacto-centric radius. This is at odds with the measured gradients in the Galaxy and chemical evolution models. To have $[CO/^{13}CO]$ and $[CO/C^{18}O]$ gradients in the right sense we are forced to favor low opacity for the CNZ and high opacity for the outer arms. However, even this is not particularly satisfying because with high $^{12}\tau$ in the arms, $[CO/C^{18}O] \simeq 300$. Moreover, if we adopt $T_{ex} \simeq 10$ K and this abundance the implied $N(H_2)$ column is almost five times that obtained using the Galactic conversion factor. Such high conversion factors may be seen in low metallicity systems, but not in solar metallicity gas (e.g., Bolatto et al. 2013)

The anomalies in the ratios demand that we consider non-LTE effects. The PDRs that were discussed in the nuclear region are not relevant in the bar arms because strong star formation is absent. Two other non-LTE effects worth considering are (1) sub-thermal excitation of the isotopologues and (2) ^{13}CO chemical fractionation in the arm medium versus the CNZ. The second we dismiss because we observe $[^{13}CO/C^{18}O]$ to be smaller than toward the CNZ. Since ^{18}O is not expected to fractionate efficiently in the cold ISM, fractionation would act to raise the $[^{13}CO/C^{18}O]$ abundance ratio relative to the nucleus, not lower it. Moreover, detailed studies find little evidence for ^{13}CO fractionation actually being observed in the ISM (e.g., Milam et al. 2005).

Sub-thermal excitation is a viable explanation, especially since the clouds in the arms likely have lower densities than the nuclear disk. The large opacity of CO lowers its effective critical density relative to the CO isotopologues by the escape probability factor ($\beta \sim 1/^{12}\tau$). Therefore when gas densities drop below $\sim n_{H_2} \leqslant 10^{3.5}$ cm^{-3}, the brightness temperatures of the CO isotopologues can drop relative to CO, inflating $\mathbb{R}_{13}$ and $\mathbb{R}_{18}$ (Meier & Turner 2001). This agrees with the observed behavior only if the true $\mathbb{R}_{13}$ and $\mathbb{R}_{18}$ are unity ($^{12}\tau \to \infty$).

If we adopt the $^{12}\tau \simeq 80$ solution for the end of the northern arm, the lowest that keeps the correct sense of the abundance gradient, then $[CO/^{13}CO] \simeq 110$ and $[CO/C^{18}O] \simeq 225$. For an excitation temperature of 10 K, the observed ^{13}CO and $C^{18}O$ intensities imply areal filling factors of $f_a \sim 0.03$. This is reasonable for the bright, extended molecular gas disk characteristic of IRAS 04296. Adopting the above abundances and temperature for the arm, $N(H_2) \simeq 3.8 \times 10^{22}$ cm^{-2} at the outer end of the northern arm. This column is larger than that from a Galactic conversion factor but is not extreme; we will use it to estimate abundances toward the northern arm. Until $J = 2$–1 transitions are observed so the gas excitation can be directly measured, implied conversion factors must be regarded as suspect, but it is clear that the conversion factor for the CNZ is lower than in the arms (Meier et al. 2010), as it is in many galactic centers.

4.1.3. CO Isotopologues and Stellar Processing in IRAS 04296

We have seen that CO isotopic abundance ratios in IRAS 04296 are anomalous compared to the Galaxy and other local galaxies. The observations further show that the physical conditions of the molecular gas in the arms are very different from that observed in the CNZ. Taking into account gas columns, absolute abundance ratios, and their variation with galactocentric radius, we conclude that $^{12}\tau \sim 4$–6, $[CO/^{13}CO] \simeq 60$ and $[CO/C^{18}O] \simeq 200$ toward the CNZ. At the outer end of the bar arm these values have changed to ~ 80, 110, and 225, respectively. The $[CO/C^{18}O]$ ratios are fairly low, consistent with the inner Galaxy value and with enrichment from massive star ejecta over much of the inner $r \sim 3.5$ kpc. However, the inner disk $[CO/^{13}CO]$ values are like those $\gtrsim 10$ kpc out in the Galactic disk. Recent observations suggest high ^{12}C to ^{13}C isotopic abundance ratios of $[^{12}C/^{13}C] \sim 100$ may be common in other starburst nuclei (Martín et al. 2010; Henkel et al. 2014). Hence, if $[CO/C^{13}O]$ can be a proxy of longer term nucleosynthetic processing, the underlying disk of IRAS 04296 and possibly other starbursts are less processed than most of the Galaxy.

Meier et al. (2010) concluded from the molecular gas and dynamical masses that IRAS 04296 must be experiencing one of its first major starburst episodes. The isotopic abundances agree with this initial burst scenario, but also show that the current burst is mature enough to have enriched the nuclear disk and potentially the inner bar with massive star ejecta. In this picture IRAS 04296's evolutionary state parallels the Large Magellanic Cloud (LMC): a relatively unprocessed galaxy with a current burst of massive star formation. However, the LMC appears to have a completely different abundance pattern, being somewhat enriched in ^{13}CO, extremely depressed in $C^{18}O$ (e.g., Wang et al. 2009), and with no sign of local isotopologue variation across the galaxy (A. Hughes et al. 2014, in preparation). Finding the metallicity of IRAS 04296 could help determine the stage of enrichment.

4.2. The Dense Molecular Gas Component in IRAS 04296

CO(1–0) is a good tracer for overall molecular gas morphology, but it is the dense gas from which stars form. We need to observe molecular species with higher critical densities than CO(1–0) to find the state and characteristics of the star forming component of molecular gas. HCN(1–0) is an example of a dense gas probe that linearly correlates with star formation rate (SFR; Gao & Solomon 2004). Other dense gas probes include HCO$^+$, HNC, CS, HC$_3$N, and CN. Here we investigate

the nature of the dense gas as traced by these species and their connection with the SFR.

4.2.1. CO(1–0)/HCN(1–0) and the Dense Gas Fraction

Since CO(1–0) traces low density molecular gas and HCN(1–0) high density, the CO(1–0)/HCN(1–0) line ratio is a measure of the fraction of gas that is dense. The tight correlation observed between HCN(1–0) and the SFR (Section 4.2.3), together with the compactness of nuclear star formation in IRAS 04296 (Meier et al. 2010), suggests that the dense gas fraction ought to increase toward the starburst.

This is indeed seen across the CNZ, with CO(1–0)/HCN(1–0) decreasing from $\geqslant 12$ at the outer edge of the nuclear disk to ~ 7 at the starburst. Just southwest of the starburst the ratio even drops below six, at the low end of that found by (single-dish) surveys of nearby [U]/LIRGs (e.g., Solomon et al. 1992; Aalto et al. 1995; Gao & Solomon 2004; Baan et al. 2008). Even averaged over the inner 20″ diameter, (close to single-dish sampling scales), the CO(1–0)/HCN(1–0) line ratio is <8. We see that the fraction of dense molecular gas, $n_{H_2} \gtrsim 10^{4.5}$ cm^{-3}, in the CNZ is high near the nuclear starburst, and falls away from the starburst.

Along the arms HCN(1–0) is only tentatively detected in a few locations (see Figure 5), so there are just a few isolated regions with elevated dense gas fractions. Given the much fainter CO(1–0) at these arm locations, they have CO(1–0)/HCN(1–0) limits that are comparable to or slightly higher than the starburst values. However, the CO isotopologues are likely better tracers of gas column (Section 4.1). If $^{13}CO/HCN$ or $C^{18}O/HCN$ is used to constrain the dense gas fraction, then there is a pronounced decrease in the dense gas fraction between the CNZ and the bar arms, as expected given the lower star formation rate there.

4.2.2. Dense Gas Properties of the Circum-nuclear Zone

Line ratios between HCN(1–0), HCO$^+$(1–0), HNC(1–0), and CN(1–0; 3/2–1/2) depend on gas physical conditions as well as chemistry. The dominant physical and chemical processes controlling the line intensities of these transitions have been extensively discussed in Paper II (Meier & Turner 2012) and the literature (e.g., Aalto et al. 2002; Graciá-Carpio et al. 2006; Meijerink et al. 2007; Papadopoulos 2007; Baan et al. 2008; Krips et al. 2008; Loenen et al. 2008; Kazandjian et al. 2012), so here we only briefly summarize.

The first-order physical parameter controlling these ratios is gas density. The critical density of HCO$^+$(1–0) is nearly an order of magnitude lower than HCN(1–0), while HNC(1–0) has a critical density slightly lower than HCN(1–0). Therefore in the density range from 10^{4-6} cm^{-3}, the HCN/HCO$^+$ depend on gas density, with HCO$^+$ favored at lower densities relative to HCN. Furthermore, HCO$^+$, being a molecular ion, has its abundance decreased in high density gas due to faster recombination with electrons (e.g., Papadopoulos 2007). Together these two effects suggest that HCN should be significantly brighter than HCO$^+$ in high density gas. In normal gas phase chemistry the HCN/HNC intensity ratio is driven to unity through the mutual formation reaction HCNH$^+$ + e$^-$ → HNC/HCN + H (e.g., Talbi & Herbst 1998; Shiba et al. 1998). In environments that are hot or have experienced strong shocks or PDR irradiation, HNC can be rapidly converted to HCN so this ratio can deviate significantly from unity (e.g., Schilke et al. 1992; Turner et al. 1997). Thus we expect HCN/HNC intensity ratios to be near unity over a wide range of high density gas conditions. Where
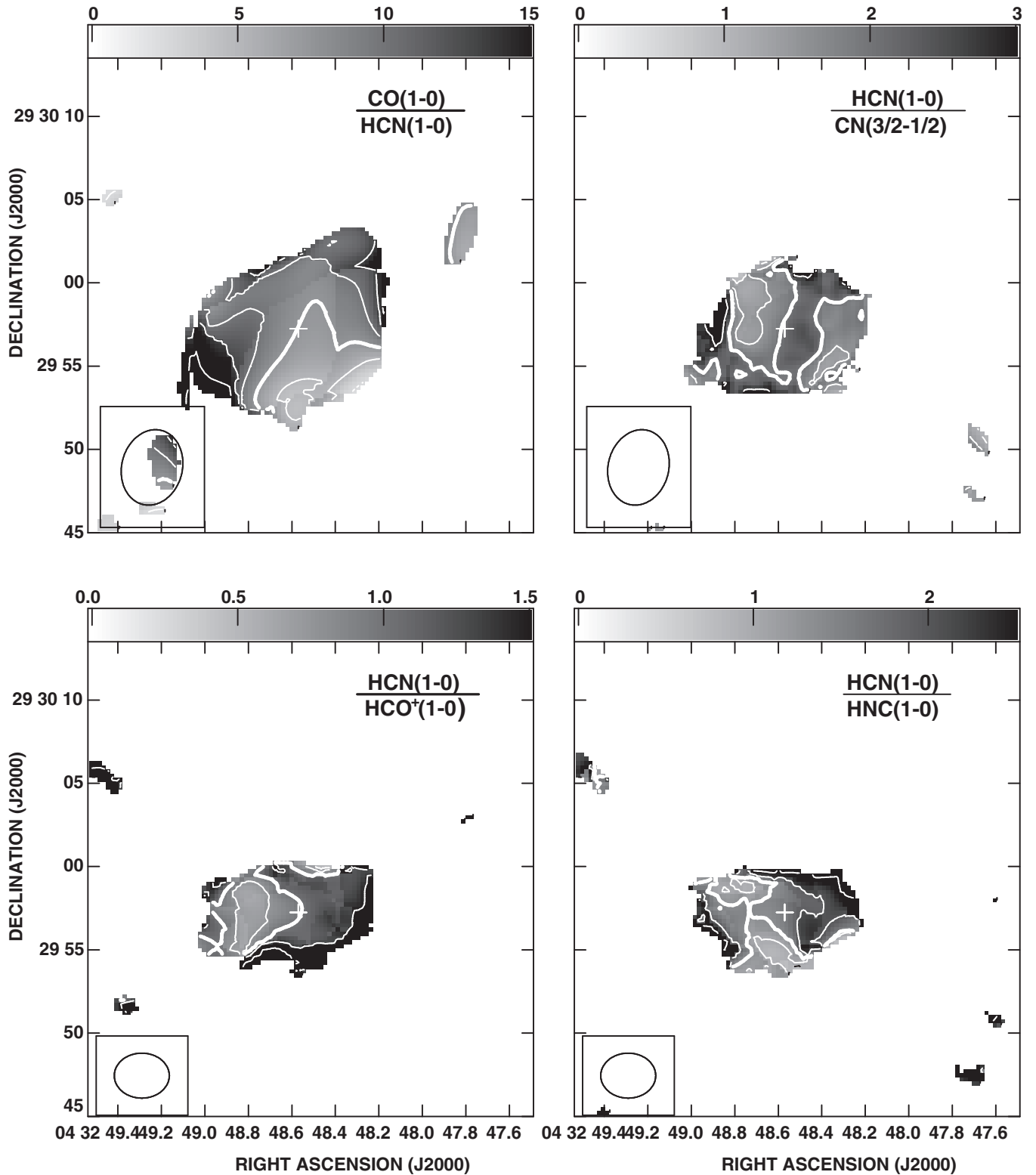
Figure 5. Intensity ratios for dense gas tracers. Top Left: CO(1–0)/HCN(1–0) line ratio. Contours are 5, 7.5 (bold contour), 10, 13.3, and 20. The grayscale ranges from 0 to 15. In all planes, darker grayscales correspond to higher ratios. Top Right: the HCN(1–0)/CN(1–0; 3/2–1/2) line ratio. Contours are 1.25, 1.5, 2.0 (bold contour), and 3.0, with grayscale ranging from 0 to 3. Bottom Left: HCN(1–0)/HCO$^+$(1–0) line ratio. Contours are 0.563, 0.75, 1.0 (bold contour), 1.5, and 3.0. The grayscale ranges from 0 to 1.5. Bottom Right: HCN(1–0)/HNC(1–0) line ratio. Contours are 0.75, 1.0, 1.33 (bold contour), 2.0, and 4.0. The grayscale ranges from 0 to 2.5. In all planes, the cross marks the location of the starburst (peak of the cm radio continuum Meier et al. (2010). The beam for the ratios is displayed in the bottom left.

deviating from unity we expect HCN to be strongly favored in hot, disturbed gas. This is generally consistent with what we observe toward the more moderate starbursts, IC 342 and Maffei 2 in Papers I and II (Meier & Turner 2005, 2012). CN is expected to trace PDR gas and its chemistry is discussed in more detail in Section 4.2.4. Finally it should be noted that high optical depth in these lines will act to hide any differences in the physical and chemical behavior, driving all the ratios to unity.

Ratios of these three transitions are displayed in Figure 5. Both the HCN(1–0)/HCO$^+$(1–0) and HCN(1–0)/HNC(1–0) line ratios exhibit the same east—west gradient across the CNZ, with high values at the western side. HCN(1–0)/HCO$^+$(1–0) ranges from 0.7 to 1.5 and HCN(1–0)/HNC(1–0) from 1.3 to 2.5. The nuclear starburst resides approximately in the middle of the observed ratio gradient in both cases, so no clear evidence is seen for a distinct component directly associated with the compact starburst. The fact that the HCN/HCO$^+$ intensity ratio is 1.0 toward the starburst suggests that densities are high enough to thermalize both transitions and that the opacities of both lines could be high. Large velocity gradient modeling of HCN (see Meier et al. 2008, for model) and HCO$^+$ toward the starburst (not shown) imply that for a kinetic temperature of 40 K (the dust temperature; Table 1) densities are $\sim 2 \times 10^5$ cm^{-3}. The inferred HCN abundance (Table 3) is near that typically observed on large scales toward star forming clouds (e.g., Blake et al. 1987), so HCN opacities, while probably >1, are unlikely to be extreme.

Both HCN/HCO$^+$ and HCN/HNC have the same sense of trend, rising toward the west across the CNZ. One possible model for these ratios is that the gas density is lower in the east away from the starburst, resulting in lower HCN/HCO$^+$ there, and warm PDR or shocked gas is more prevalent in the west near the starburst, favoring HCN emission and producing the high HCN/HNC line ratio there. The starburst and CO column density peak, is located at the inner terminus of the northwestern bar arm, suggesting the western side of the nucleus to be hotter/more energetic (Meier et al. 2010). In this model, the elevated HCN/HCO$^+$ is a better indicator of high gas density and HCN/HNC more reflective of high radiation fields. However opacity must also be considered. A second possible model is that line ratios near the starburst could instead be dominated by high HCN line opacity; if HCN is opaque but the two lower abundance species, HCO$^+$ and HNC, transition from optically thick to thin from west to east, following the decline in CO column, then the decline in HCO$^+$ and HNC brightness relative to HCN toward the east could be explained by their decline in opacity in this region. However, this second model is less favored since HCN/HCO$^+$ (and HCN/HNC) on the western side are significantly above one, ratios naively inconsistent with high opacities.

4.2.3. HCN(1–0) and the Nuclear Star Formation Rate

Here we consider IRAS 04296, a spatially resolved LIRG, in the context of the global L_{IR} versus HCN(1–0) relations (e.g., Gao & Solomon 2004; Garcia-Burillo et al. 2012). The total HCN(1–0) luminosity over the CNZ is $L_{HCN} = 7.4 \times 10^7$ K km s^{-1} pc^2. This equates to $L_{IR}/L_{HCN} = 1300$ $L_\odot$ (K km s^{-1} pc^2). This value is 1.5 times the global values of [U]LIRGs (Gao & Solomon 2004; Garcia-Burillo et al. 2012, with $L_{IR} \simeq 10^{11} L_\odot$). However, the IR fluxes from IRAS cover a much larger area than the HCN emission. If we adopt L_{IR}(CNZ) $\simeq 0.5$ L_{IR}(tot) (Meier et al. 2010), then the observed nuclear value for IRAS 04296 is $L_{IR}/L_{HCN} = 660$, which is 40%

smaller than the global values. That the CNZ in IRAS 04296 is slightly IR under-luminous normalized by the HCN compared to global averages is consistent with the determination focused tightly on the dense gas of the CNZ region.

Since HCN(1–0) is imaged at high resolution, a rough estimate is attempted to see if the correlation also persists within the galaxy. Meier et al. (2010) provide a detailed discussion of the rate, efficiency and distribution of star formation over the nucleus of IRAS 04296. However, the high frequency radio data does not sample the SFR on spatial scales comparable to HCN(1–0) and so we use a cruder SFR proxy, the 20 cm radio continuum map. Figure 3 displays the 20 cm radio continuum (Meier et al. 2010) compared with HCN(1–0) at matched spatial resolution. There is a clear linear correlation between the two. Adopting a q parameter value of 2.3 ($q = \log[L_{FIR}/3.75 \times 10^{12} W/m^2] - \log[S_{20cm}/10^{26} Jy]$), typical of what is commonly observed for star forming galaxies (Condon 1992), the observed L_{IR}/L_{FIR} ratio (with L_{IR} being the total luminosity from 8 to 1000 μm and L_{FIR} being the luminosity from 40 to 400 μm; Sanders et al. 2003), and Gao & Solomon (2004)'s conversion between L_{IR} and SFR allows the 20 cm map to be roughly converted to a resolved SFR map. The observed correlation between HCN(1–0) and 20 cm radio continuum intensity is

$$I_{20}(mJy\,bm^{-1}) = [0.38 \pm 0.08]I_{HCN}(K\,km\,s^{-1}) - [0.42 \pm 0.35]. \quad (2)$$

For the above normalization, after converting intensities to fluxes and luminosities, we find

$$SFR(M_\odot\,yr^{-1}) = [1.4 \pm 0.3 \times 10^{-7}]L_{HCN}(K\,km\,s^{-1}\,pc^2) - [0.02 \pm 0.02]. \quad (3)$$

The quoted errors are statistical only and do not include (potentially large) systematic errors associated with uncertainties in adopted q and the conversion between L_{IR} and SFR. Discounting the very small zero-point offset, we find a slightly lower normalization than the SFR($M_\odot$ yr^{-1}) = (1.8×10^{-7}) L_{HCN}(K km s^{-1} pc^2) value of Gao & Solomon (2004). Given the assumptions this is considered good agreement between the local and global values.

HCO$^+$, which has a critical density lower than HCN's, shows a statistically identical relationship. Krumholz & Thompson (2007) suggest that the slope and normalization of the SFR vs. molecular gas tracer relationship should differ between species that are fully thermalized and those that are not. The fact that we do not see a difference is further evidence that the molecular gas localized to the starburst in IRAS 04296 has a density high enough to excite both HCN(1–0) and HCO$^+$(1–0) equally well over much of the CNZ and that both may have moderate opacity. This finding is consistent with other observations of dense gas tracers in nearby, resolved star-forming galaxies (Zhang et al. 2014).

4.2.4. PDRs and the Nuclear Starburst in IRAS 04296

The interaction of UV photons from the starburst's massive stars with the molecular gas is expected to result in PDRs with distinctive chemical properties (e.g., Tielens & Hollenbach 1985; Sternberg & Dalgarno 1995). Given the strong nuclear star formation in IRAS 04296, does it show signs of radiative feedback from the starburst in the gas chemistry?

CN is expected to be abundant in PDRs. It forms from reactions between CH and N, with CH forming directly from H$_2$ and PDR-abundant C$^+$(Sternberg & Dalgarno 1995). CN(1–0;

3/2–1/2) and HCN(1–0) have similar critical densities, so the HCN(1–0)/CN(1–0; 3/2–1/2) (hereafter HCN(1–0)/CN(1–0)) line ratio is considered to be an excellent tracer of dense PDRs (e.g., Sternberg & Dalgarno 1995; Boger & Sternberg 2005).

Toward the starburst in IRAS 04296 the HCN(1–0)/CN(1–0) line ratio reaches 2.4, which for LTE corresponds to an [HCN/CN] abundance ratio of $\geqslant 0.6$ and a CN abundance of 9.0×10^{-9}. (The abundance ratio is a lower limit because of the potentially large HCN opacity, whereas it is shown in Section 3 that CN is optically thin.) According to the models of Boger & Sternberg (2005), the above conditions are consistent with molecular gas at $A_V \simeq 4$–5 mag and a range of densities and radiation fields, χ. In the range $A_V \sim 4$–6 the predicted column ratio changes dramatically (Boger & Sternberg 2005), so the implied A_V is not strongly sensitive to the optical depth of HCN as long as it is <10. Moderate densities ($\leqslant 10^4 \mathrm{cm}^{-3}$) and radiation fields ($\chi < 10^3$), where χ is the normalized Draine solar neighborhood radiation field at 1000 Å are slightly favored since as density and χ increase, peak CN abundances drop below 10^{-8} as ionization is pushed deeper into the cloud. Molecular gas at $A_V \simeq 4$–5 corresponds roughly to the transition between PDR and dark cloud conditions. So the starburst ISM traced by CN and HCN in IRAS 04296 appears to be influenced by PDRs, but not strongly. Furthermore, the fact that the HCN(1–0)/HNC(1–0) ratio > 1 over the CNZ favors PDR conditions. Localized chemical effects associated with X-ray dominated regions such as from a buried active galactic nucleus (AGN) are not pronounced (e.g., Meijerink et al. 2007).

To explain the total observed CN column density when $n_{H_2} \leqslant 10^4 \mathrm{cm}^{-3}$ and $\chi \lesssim 10^3$ with $A_V \sim 4$–5 gas requires ~ 45 PDR clouds along the line of sight. Using the same observed ratio, Boger & Sternberg (2005) and Fuente et al. (2005) estimate somewhat higher χs for the giant PDR in M 82, but fewer (10–20) numbers of PDR clumps. The number of clumps estimated here is 2–4 times larger than for M 82, the same factor by which the SFR is larger.

However, it is hard to explain why HCN(1–0)/CN(1–0) decreases toward the outer CNZ in the context of PDR gas. This implies that the abundance of the PDR tracer CN relative to HCN increases with distance from the starburst, contrary to expectation. One possible explanation is that the ionization remains high over the entire CNZ, via the weaker extended star formation component or elevated cosmic ray ionization rate and the gas away from the starburst being on average somewhat more diffuse. This model of more diffuse gas in the outer CNZ, away from the starburst, is also consistent with the lower HCN(1–0)/CO(1–0) ratio there, since diffuse clouds have lower total dense gas fractions.

4.3. Gas-grain Chemistry Across IRAS 04296

CH$_3$OH and HNCO have no efficient gas-phase pathway but are easily formed on grain mantles. Large gas-phase abundances of these species require mantle disruption, either by evaporation or shocks. CH$_3$OH is observed to peak just north of the starburst. Here CH$_3$OH abundances reach 1.8×10^{-8} (Table 3). HNCO is tentatively detected toward the CNZ, with an abundance of $\sim 2.3 \times 10^{-9}$. Both are highly elevated relative to abundances in quiescent molecular clouds in the Galaxy (Kalenskii et al. 1997; Minier & Booth 2002) and comparable to the abundances observed on giant-molecular-cloud scales toward the strongest shock regions in nearby galaxies (e.g., Meier & Turner 2005, 2012).

Since the SFR is large toward the starburst, we investigate whether the nuclear CH$_3$OH intensity can be explained by large collections of compact sources such as proto-stellar outflows or hot cores (e.g., Usero et al. 2006). We estimate the CH$_3$OH intensity produced from molecular outflows by taking the size and CH$_3$OH brightness of the proto-typical molecular outflow, L1157 (Bachiller & Pérez-Guitiérrez 1997). At the distance of IRAS 04296, we estimate a single such outflow will contribute an intensity, $I(\mathrm{CH_3OH})_{\mathrm{out}} \sim 1.3 \times 10^{-6} \mathrm{K \, km \, s}^{-1}$. To reproduce the observed intensity (Figure 2), we require 3.2×10^7 such outflows, or 290 outflows pc^{-2}. The surface density of outflows predicted from a Salpeter IMF ($M_u = 100 \, M_\odot$; $M_l = 0.1 \, M_\odot$), a lifetime of 10^{-4} yr, and a SFR of $12 \, M_\odot \mathrm{yr}^{-1}$ (Meier et al. 2010), is 3.1 outflows pc^{-2}, that is, two orders of magnitude too low to explain the observed methanol emission. The situation is even more untenable for HNCO (Rodríguez-Fernández et al. 2010). Hot molecular cores cannot either, which are roughly as common as outflows but an order of magnitude smaller in angular size, match the observed abundances.

Therefore we conclude that only (large-scale) shocks are capable of explaining the observed abundances and that CH$_3$OH provides a mapping of those shocks across the galaxy. This agrees with what is seen in local starburst galaxies (Meier & Turner 2005, 2012). Clearly, the CNZ is a site of strong dynamical shocks. That the CH$_3$OH peaks off of the starburst could reflect shocks associated with the intersection of the inner molecular arms with the CNZ, as is observed in nearby bars (Meier & Turner 2005, 2012). It is also possible that the weakness of CH$_3$OH at the starburst is due to depopulation of the low lying energy states or to direct photo-dissociation.

Toward the end of both bar arms we tentatively ($\sim 4\sigma$ in the north and $\sim 3\sigma$ in the south) detect CH$_3$OH emission. CH$_3$OH abundances toward these locations are comparable to those seen toward the CNZ. CH$_3$OH is similarly enhanced at the end of nuclear bar of the nearby starburst Maffei 2, suggesting that the structure of the (large-scale) bar here resembles the *nuclear* bar in Maffei 2 (Meier & Turner 2012). Shocks have been proposed as a deterrent to star formation along the arms, allowing gas to drift into the nuclear starburst region (Meier et al. 2010). CH$_3$OH emission is not detected elsewhere in the inner bar arms, but limits on its abundance ($<1.8 \times 10^{-8}$) are inconclusive. So the observations do not rule out the existence of such strong shocks along the inner arms.

The tentative detection of HNCO toward the nuclear disk permits a limit to be placed on the HNCO(5_{05}–4_{04})/CH$_3$OH(2_k–1_k) line ratio. As discussed in Meier & Turner (2012), the HNCO/CH$_3$OH line ratio is sensitive to the physical conditions present in the shocked gas. This ratio is sensitive both to photodissociation and gas density. HNCO is both more rapidly photodissociated (e.g., Martín et al. 2009) and the observed transition has a slightly higher critical density than CH$_3$OH. Toward the nuclear disk, HNCO/CH$_3$OH ~ 0.25, while toward the northern bar arm, HNCO/CH$_3$OH < 0.20. These ratios are small compared to those observed on small scales in the moderate star formation rate nuclear bars, IC 342 and Maffei 2 (0.9–1.1; Meier & Turner 2005, 2012), but comparable to the limits in M 82 (Martín et al. 2006; Aladro et al. 2011b). Hence the low HNCO/CH$_3$OH ratio suggests that either densities are on average lower or shocked gas is more strongly penetrated by UV radiation in the IRAS 04296 CNZ than in the nuclear bars of normal spiral galaxies. The brightness of the dense gas tracers toward the CNZ argues against the former explanation and the strong starburst favors the latter. However the latter is in some

tension with the modest implied PDR penetration (Section 4.2.4). Away from the starburst, at the end of the bar, lower gas density may be the reason for the low HNCO/CH$_3$OH intensity ratio.

4.4. IRAS 04296 Nuclear Physical Conditions Compared to Nearby Starbursts

Extensive recent work has focused on the dense gas properties of nearby, strong starbursts (e.g., Henkel et al. 1991; Nguyen-Q-Rieu et al. 1992; Solomon et al. 1992; Kohno et al. 2001; Aalto et al. 2002; Gao & Solomon 2004; Graciá-Carpio et al. 2006; Pérez-Beaupuits et al. 2007; Imanishi et al. 2007; Krips et al. 2008; Bussmann et al. 2008; Baan et al. 2008; Graciá-Carpio et al. 2008; Juneau et al. 2009; Bayet et al. 2009; Jiang et al. 2011; Garcia-Burillo et al. 2012). Here we place the dense gas properties of IRAS 04296 in the context of these studies.

The CNZ intensity ratios, CO/HCN $\sim$ 7, HCN/HCO$^+$ $\sim$ 1.0, HCN/HNC $\sim$ 1.3, and HCN/CN $\sim$ 2.0 fall well within the range found for other luminous starburst galaxies. The CO/HCN ratio lies at the low end of the range, and the HCN/CN ratio lies at the high end of the range, while HCN/HCO$^+$ and HCN/HNC are more typical (e.g., Baan et al. 2008). The limit on the HC$_3$N/HCN line ratio of 0.086 is very similar to the ratio found for NGC 253 (e.g., Lindberg et al. 2011; Baan et al. 2008). So either IRAS 04296 does not have a strongly enhanced very high density gas component or elevated excitation moving population up out of these intermediate J-level HC$_3$N transitions plausibly explains the observed faintness of this 3 mm line (Mauersberger et al. 1990; Meier et al. 2011; Meier & Turner 2012).

The dense gas line ratios observed toward IRAS 04296's starburst are similar to those observed with single-dish telescopes toward the starburst in NGC 253, except that the CO/HCN line ratio in IRAS 04296 is $\sim$3 times lower than NGC 253's single-dish value and the HCN/CN is a factor of four larger (e.g., Baan et al. 2008). However, the CO/HCN line ratio toward NGC 253 measured at the $\sim$3$''$ approaches that of IRAS 04296 (Knudsen et al. 2007). Therefore the higher single-dish CO/HCN ratio in NGC 253 is likely an artifact of more diffuse gas being included in the single-dish beam compared to IRAS 04296. The comparatively faint CN indicates that the starburst ISM in IRAS 04296 has not been penetrated by PDRs to quite the degree of NGC 253.

The higher HCN/CN intensity and the higher dense gas fraction suggests that the starburst in IRAS 04296 is at an early stage of evolution. Baan et al. (2010) generate simple decaying starburst models to track the evolution of the dense component in a starburst. They use the model to simultaneously predict the CO/HCN intensity ratio and L_{IR}. IRAS 04296's CO/HCN and L_{IR} place its burst at the earliest phases ($\tau_{age} \leqslant 5 \times 10^6$ yr.) This interpretation is also consistent with the CO isotopologue data. Meier et al. (2010) have concluded that the starburst is not sustainable, a true burst, based on the fact that the nuclear gas consumption time is much shorter than the gas inflow rate along the bar, and that it must be a young starburst since molecular mass constitutes $\sim$25–30% of the dynamical mass in the CNZ (Table 1).

The morphological similarity between NGC 253 and IRAS 04296 is strong. Both are strongly barred spirals with starbursts triggered by bar-driven inflow. The nuclear starbursts in both IRAS 04296 and NGC 253 are close cousins, with IRAS 04296's burst being somewhat more intense, at an earlier phase and residing in a possibly less processed disk.

5. CONCLUSIONS

We have imaged emission from lines of dense gas tracers at 3 mm with OVRO and CARMA toward the nearby LIRG, IRAS 0496+2923. The images have 3$''$ to 4$''$.5 spatial resolution, and cover the central arcminute region ($\sim$8.4 kpc in diameter). We have combined these data with archival OVRO CO data to study chemical effects of an intense nuclear starburst, SFR $\sim$ 10 $M_\odot$ yr^{-1}, on its gas.

1. We confirm that IRAS 04296 is one of the brightest molecular line-emitting galaxies in the sky. We detect significant emission in CO(1–0), ^{13}CO(1–0), C^{18}O(1–0) HCN(1–0), HNC(1–0), HCO$^+$(1–0), CN(1–0; 3/2–1/2), CN(1–0; 1/2–1/2), and CH$_3$OH. Gas properties in IRAS 04296 are similar to those in the starburst galaxy NGC 253, although IRAS 04296 is more gas-rich.

2. Emission from the dense gas tracers, HCO$^+$, HNC, and CN, is primarily confined to the inner $R \sim 500$ pc (5$''$) CNZ, and requires densities of $n \gtrsim 2$–10×10^4cm^{-3} here. It is within this component that the starburst is located. The CO/HCN ratio in IRAS 04296 is $\sim$6–8 for the inner $R < 500$ pc region, and $\geqslant$12 in most locations within the arms. This ratio traces the fraction of molecular gas that is dense, indicating nearly a factor of two higher dense-gas fraction in the nucleus as compared to the arms (though two locations in the arms have CO/HCN ratios comparable to the nucleus).

3. The three CO isotopic lines, which trace less dense gas, are detected across the central $R \sim 5$–6 kpc ($\sim$40$''$) diameter. $\mathbb{R}_{13}$, the CO(1–0)/^{13}CO(1–0) line ratio, $= 16 \pm 4$ in the CNZ ($R < 500$ pc) of IRAS 04296 and falls to the very low value of 1.9 ± 0.4 by the outer end of the bar. The higher-than-Galactic $\mathbb{R}_{13}$ in the CNZ is consistent with observations of other actively star-forming galaxies. ^{12}CO(1–0)/C^{18}O(1–0), $\mathbb{R}_{18}$, follows the same pattern with $\mathbb{R}_{18} = 45 \pm 10$ in the nuclear starburst–CNZ and falling to 3.3 ± 0.7 toward the outer disk. This trend is likely due to either lower opacities in CO due to kinematics or to higher excitation temperature in the CNZ, which removes molecules from the lowest CO rotational levels.

4. The intensity ratio ^{13}CO(1–0)/C^{18}O(1–0) or $\mathbb{R}_{1318}$ is low, $\mathbb{R}_{1318} = 3.2 \pm 0.8$, in the CNZ, and even lower in the outer bar, with $\mathbb{R}_{1318} \lesssim 2$. Interpretation of this unprecedentedly low ratio in terms of very high CO opacities conflicts with the high observed CO(1–0)/^{13}CO(1–0). We can obtain barely consistent solutions for the CO isotopic ratios if we adopt [CO]/[^{13}CO] $\sim$ 60 toward the nucleus of IRAS 04296, increasing to 110 at the bar ends, and [CO]/[C^{18}O] $\sim$ 200–225. These values may indicate a relative lack of long term stellar processing in IRAS 04296 as compared to the Galaxy. For the implied isotopic abundance ratios, optically thin C^{18}O(1–0) emission predicts a nuclear conversion factor $\sim$0.5 times that of the Galactic disk. The implied conversion factor in the bar arms are approximately equal (or slightly larger) than in the Galactic disk, consistent with that found in Meier et al. (2010).

5. The observed global value of $L_{IR}/L_{HCN} \simeq 1300 \, L_\odot$ (K km s^{-1} pc^2) obtained for IRAS 04296 is nearly a factor of 1.5 times the standard global value for the IR to HCN luminosity ratio obtained by Gao & Solomon (2004). Excluding the non-CNZ IR luminosity, we obtain a value for the CNZ alone of $L_{IR}/L_{HCN} \simeq 660 L_\odot$ (K km s^{-1} pc^2) for IRAS 04296. From this we estimate a star formation rate

relation $SFR(M_\odot\,yr^{-1}) = 1.4 \pm 0.3 \times 10^{-7}\,L_{HCN}$, similar given the large systematic uncertainties, to that obtained by Gao & Solomon.

6. From LTE analysis we find that the CN abundance is $\sim$1.6 times the abundance of HCN, if HCN is optically thin. If HCN is optically thick then HCN can still be more abundant than CN. Based on the models of Boger & Sternberg (2005) the HCN/CN column density ratio indicates that the emission is coming from clouds at moderate depths of $A_v \sim 4$. This corresponds to the transition between PDRs and dark clouds. So the CNZ is moderately influenced by PDRs. The HCN/CN ratio decreases radially from the starburst in the CNZ. This may suggest that PDR-influenced gas extends well beyond the compact starburst coupled with a drop in characteristic A_v.

7. Bright emission from the CH$_3$OH molecule indicates that grain chemistry is important on large scales in IRAS 04296. We are unable to reproduce the emission from models of collections of compact sources, and conclude that only a widespread mechanism such as shocks along spiral arms can explain the observed brightnesses of these species. A tentative detection of CH$_3$OH at a galactocentric radius of > 2 kpc is presented. The CH$_3$OH abundance in this region are comparable to those found in the CNZ.

8. All lines of evidence, including the unusual CO isotopologue ratios and CO/HCN vs. L_{IR}, indicate that the starburst in IRAS 04296 is very young, which is consistent with previous suggestions based on bar-fueling of the starburst (Meier et al. 2010).

Facilities: CMA, OVRO

REFERENCES

Aalto, S., Booth, R. S., Black, J. H., & Johansson, L. E. B. 1995, A&A, 300, 369
Aalto, S., Johansson, L. E. B., Booth, R. S., & Black, J. H. 1991, A&A, 249, 323
Aalto, S., Polatidis, A. G., Hüttemeister, S., & Curran, S. J. 2002, A&A, 381, 783
Aladro, R., Martín-Pintado, J., Martín, S., Mauersberger, R., & Bayet, E. 2011a, A&A, 525, A89
Aladro, R., Martín, S., Martín-Pintado, J., et al. 2011b, A&A, 535, A84
Baan, W. A., Henkel, C., Loenen, A. F., Baudry, A., & Wiklind, T. 2008, A&A, 477, 747
Baan, W. A., Loenen, A. F., & Spaans, M. 2010, A&A, 516, A40
Bachiller, R., & Pérez-Guitiérrez, M. 1997, ApJ, 487, L93
Bayet, E., Aladro, R., Martín, S., Viti, S., & Martín-Pintado, J. 2009, ApJ, 707, 126
Blake, G. A., Sutton, E. C., Masson, C. R., & Phillips, T. G. 1987, ApJ, 315, 621
Boger, G. I., & Sternberg, A. 2005, ApJ, 632, 302
Bolatto, A. D., Wolfire, M., & Leroy, A. K. 2013, ARA&A, 51, 207
Bussmann, R. S., Narayanan, D., Shirley, Y. L., et al. 2008, ApJ, 681, L73
Casoli, F., Dupraz, C., & Combes, F. 1992, A&A, 264, 55
Chamaraux, P., Kazes, I., Saito, M., Yamada, T., & Takata, T. 1995, A&A, 299, 347
Chin, Y.-N., Henkel, C., Whiteoak, J. B., Langer, N., & Churchwell, E. B. 1996, A&A, 305, 960
Condon, J. J. 1992, ARA&A, 30, 575
Frerking, M. A., Langer, W. D., & Wilson, R. W. 1982, ApJ, 262, 59
Fuente, A., Fuente, A., García-Burillo, S., Gerin, M., et al. 2005, ApJ, 619, L155
Gao, Y., & Solomon, P. M. 2004, ApJ, 606, 271
Garcia-Burillo, S., Usero, A., Alonso-Herrero, A., et al. 2012, A&A, 539, A8
Graciá-Carpio, J., García-Burillo, S., Planesas, P., & Colina, L. 2006, ApJL, 640, L135
Graciá-Carpio, J., García-Burillo, S., Planesas, P., Fuente, A., & Usero, A. 2008, A&A, 479, 703
Henkel, C., Asiri, H., Ao, Y., et al. 2014, A&A, 565, A3
Henkel, C., Baan, W. A., & Mauersberger, R. 1991, A&ARv, 3, 47
Henkel, C., & Mauersberger, R. 1993, A&A, 274, 730
Huettemeister, S., Henkel, C., Mauersberger, R., et al. 1995, A&A, 295, 571
Hunter, S. D., Bertsch, D. L., Catelli, J. R., et al. 1997, ApJ, 481, 205
Imanishi, M., Nakanishi, K., Tamura, Y., Oi, N., & Kohno, K. 2007, AJ, 134, 2366
Jiang, X., Wang, J., & Gu, Q. 2011, MNRAS, 418, 1753
Juneau, S., Narayanan, D. T., Moustakas, J., et al. 2009, ApJ, 707, 1217
Kalenskii, S. V., Dzura, A. M., Booth, R. S., Winnberg, A., & Alakoz, A. V. 1997, A&A, 321, 311
Kazandjian, M. V., Meijerink, R., Pelupessy, I., Israel, F. P., & Spaans, M. 2012, A&A, 542, A65
Knudsen, K. K., Walter, F., Weiss, A., et al. 2007, ApJ, 666, 156
Kohno, K., Matsushita, S., Vila-Vilaró, B., et al. 2001, in ASP Conf. Proc. 249, The Central Kiloparsec of Starbursts and AGN: The La Palma Connection, ed. J. H. Knapen, J. E. Beckman, I. Shlosman, & T. J. Mahoney (San Francisco, CA: ASP), 672
Krips, M., Neri, R., García-Burillo, S., et al. 2008, ApJ, 677, 262
Krumholz, M. R., & Thompson, T. A. 2007, ApJ, 669, 289
Lindberg, J. E., Aalto, S., Costagliola, F., et al. 2011, A&A, 527, A150
Loenen, A. F., Spaans, M., Baan, W. A., & Meijerink, R. 2008, A&A, 488, L5
Martín, S., Aladro, R., Martín-Pintado, J., & Mauersberger, R. 2010, A&A, 522, A62
Martín, S., Martín-Pintado, J., & Mauersberger, R. 2006, A&A, 450, L13
Martín, S., Martín-Pintado, J., & Viti, S. 2009, ApJ, 706, 1323
Mauersberger, R., Henkel, C., & Sage, L. J. 1990, A&A, 236, 63
Meier, D. S., & Turner, J. L. 2001, ApJ, 551, 687
Meier, D. S., & Turner, J. L. 2004, AJ, 127, 2069
Meier, D. S., & Turner, J. L. 2005, ApJ, 618, 259
Meier, D. S., & Turner, J. L. 2012, ApJ, 755, 104
Meier, D. S., Turner, J. L., Beck, S. C., et al. 2010, AJ, 140, 1294
Meier, D. S., Turner, J. L., & Hurt, R. L. 2000, ApJ, 531, 200
Meier, D. S., Turner, J. L., & Hurt, R. L. 2008, ApJ, 675, 281
Meier, D. S., Turner, J. L., & Schinnerer, E. 2011, AJ, 142, 32
Meijerink, R., Spaans, M., & Israel, F. P. 2007, A&A, 461, 793
Milam, S. N., Savage, C., Brewster, M. A., Ziurys, L. M., & Wyckoff, S. 2005, ApJ, 634, 1126
Minier, V., & Booth, R. S. 2002, A&A, 387, 179
Nguyen-Q-Rieu, Q.-R., Jackson, J. M., Henkel, C., Truong, B., & Mauersberger, R. 1992, ApJ, 399, 521
Paglione, T. A. D., Wall, W. F., Young, J. S., et al. 2001, ApJS, 135, 183
Papadopoulos, P. P. 2007, ApJ, 656, 792
Pérez-Beaupuits, J. P., Aalto, S., & Gerebro, H. 2007, A&A, 476, 177
Rodríguez-Fernández, N. J., Tafalla, M., Gueth, F., & Bachiller, R. 2010, A&A, 516, A98
Sanders, D. B., Mazzarella, J. M., Kim, D.-C., Surace, J. A., & Soifer, B. T. 2003, AJ, 126, 1607
Sanders, D. B., & Mirabel, I. F. 1996, ARA&A, 34, 749
Sanders, D. B., Scoville, N. Z., & Soifer, B. T. 1991, ApJ, 370, 158
Sanders, D. B., Soifer, B. T., Elias, J. H., et al. 1988, ApJ, 325, 74
Scoville, N. Z., Carlstrom, J., Padin, S., et al. 1994, in ASP Conf. Ser. 59, Astronomy with Millimeter and Submillimeter Wave Interferometry, ed. M. Ishiguro & J. Welch (IAU Colloq. 140; San Francisco, CA: ASP), 10
Seaquist, E. R., Frayer, D. T., & Bell, M. B. 1998, ApJ, 507, 745
Shiba, Y., Hirano, T., Nagashima, U., & Ishii, K. 1998, JChPh, 108, 698
Schilke, P., Walmsley, C. M., Pineau Des Forets, G., et al. 1992, A&A, 256, 595
Soifer, B. T., Sanders, D. B., Madore, B. F., et al. 1987, ApJ, 320, 238
Solomon, P. M., Downes, D., & Radford, S. J. E. 1992, ApJL, 387, L55
Solomon, P. M., Downes, D., Radford, S. J. E., & Barrett, J. W. 1997, ApJ, 478, 144
Sternberg, A., & Dalgarno, A. 1995, ApJS, 99, 565

Strauss, M. A., Huchra, J. P., Davis, M., et al. 1992, ApJS, 83, 29
Strong, A. W., Bloemen, J. B. G. M., Dame, T. M., et al. 1988, A&A, 207, 1
Talbi, D., & Herbst, E. 1998, A&A, 333, 1007
Tielens, A. G. G. M., & Hollenbach, D. 1985, ApJ, 291, 722
Turner, B. E., Pirogov, L., & Minh, Y. C. 1997, ApJ, 483, 235
Usero, A., Garcia-Burillo, S., Martín-Pintado, J., Fuetner, A., & Neri, R. 2006, A&A, 448, 457

Wall, W. F., & Jaffe, D. T. 1990, ApJL, 361, L45
Wang, M., Chin, Y.-N., Henkel, C., Whiteoak, J. B., & Cunningham, M. 2009, ApJ, 690, 580
Wilson, T. L., & Rood, R. 1994, ARA&A, 32, 191
Woody, D. P., Beasley, A. J., Bolatto, A. D., et al. 2004, Proc. SPIE, 5498, 30
Wouterloot, J. G. A., & Brand, J. 1996, A&AS, 119, 439
Young, J. S., Xie, S., Tacconi, L., et al. 1995, ApJS, 98, 219
Zhang, Z.-Y., Gao, Y., Henkel, C., et al. 2014, ApJL, 784, L31